C_c (0.75 to 0.92) of the samples indicate that the soil is poorly graded and falls under cohesion-less category. Therefore, shear strength becomes less; angle of friction (ϕ) becomes more due to which inter-granular attraction is less and ultimately, bank erosion takes place. Therefore, bank erosion hazard at these sites need proper attention for providing effective policy decision and execution of appropriate protection measures.

1. Chatterjee, S. and Mistri, B., Impact of river bank erosion on human life: a case study in Shantipur Block, Nadia District, West Bengal. *Int. J. Humanities Social Sci. Invent.*, 2013, **2**(8), 108–111.
2. Rosgen, D. L., A practical method of computing stream bank erosion rate. In Proceedings of the 7th Federal Interagency Sedimentation Conference, USGS, Reston, VA, 2001, vol. 2, pp. 1–15.
3. Bhowmik, M. and Das (Pan), N., Qualitative assessment of bank erosion hazard in a part of the Haora River, West Tripura District. In Proceedings of the IGU, Rohtak Conference on Landscape, Ecology and Water Management (eds Singh, M., Singh, R. B. and Hassan, M. I.), Springer, Japan, 2013, vol. 2, pp. 193–203.
4. Schumm, S. A. and Dumont, J. F., *Active Tectonics and Alluvial Rivers*, Cambridge University Press, 2000, p. 276.
5. American Society for Testing and Materials (ASTM). Standard test method for particle-size analysis of soils. Designation D2487, Philadelphia, 2011.
6. Laskar, A. and Phukon, P., Erosional vulnerability and spatio-temporal variability of the Barak River, NE India. *Curr. Sci.*, 2012, **103**(1), 80–86.
7. Shrestha and Tamrakar, Bank erosion process and bank material loss potential in Manahara River, Kathmandu, Nepal. *Bull. Depart. Geol.*, 2007, **10**, 33–44.
8. Connecticut River Joint Commissions, River dynamics and erosion. Lebanon, 1996, 1, p. 3.
9. Thorne, C. R., Processes and mechanisms of river bank erosion. In *Gravel-bed Rivers: Fluvial Processes, Engineering and Management* (eds Hey, R. D., Bathurst, J. C. and Thorne, C. R.), John Wiley, New York, 1982, pp. 227–271.
10. Thorne, C. R., Bank erosion and meander migration of the Red and Mississippi Rivers, USA. In Proceedings of the Vienna Symposium on Hydrology for Water Management of Large River Basins, 1991, pp. 301–313.
11. American Society for Testing and Materials (ASTM). Standard test method for particle-size analysis of soils. Designation D422-63, Philadelphia, 2007.
12. Mamo, B. G., Banoth, K. K. and Dey, A., Effect of strain rate on shear strength parameter of sand. In Proceedings of the 50th Indian Geotechnical Conference, Pune, India, 2015.
13. Baishya, S. J., A study on bank erosion by the River Baralia (Bhairatolajan) in Melkipara Village of Hajo Revenue Circle, Kamrup District, Assam, India. *Int. J. Sci. Res. Publ.*, 2013, **3**(9), 1–10.
14. Terzaghi, K. and Peck, R. B., *Soil Mechanics in Engineering Practice*, John Wiley, New York, 1967, p. 729.

ACKNOWLEDGEMENT. We thank the Department of Science and Technology (SERB), Government of India for providing financial help for this work.

Received 9 December 2016; revised accepted 23 July 2018

doi: 10.18520/cs/v115/i8/1571-1576

Garnetiferous metamorphic rocks in Jaspa granite, Himachal Pradesh, India: implication of Tethyan Himalayan metamorphism and tectonics

S. S. Thakur*, A. K. Singh, D. Rameshwar Rao, Rajesh Sharma, Subhajit Pandey and Aliba Ao

Wadia Institute of Himalayan Geology, 33 GMS Road, Dehradun 248 001, India

Studies on the magmatic enclaves, pelitic xenoliths and host Jaspa granite pluton outcropped in the Lahaul area, NW Himalaya, India illustrate that the rocks have undergone garnet-grade metamorphism. The *P–T* pseudosection modelling shows that the metamorphic mineral assemblage is stable in the *P–T* range ~4.5–7.3 kbar and ~440–500°C, matching quite well with the results obtained from the conventional geothermobarometers (5.7–8.6 kbar and 409–531°C). The observed garnet-grade metamorphism in and around the Jaspa pluton is proposed to be due to localized perturbation of high-temperature isotherms in the Tethys Himalaya, as a consequence of the Cenozoic tectono-thermal event during Himalayan orogeny. Further, the Haimanta group of Tethys Himalayan rocks in the Lahaul area has been interpreted to have attained right-way-up metamorphic field gradient.

Keywords: Garnet-grade metamorphism, granite pluton, magmatic enclaves, pelitic xenoliths.

THE Tethys Himalaya Sequence (THS) forms an important lithotectonic unit of the Himalayan orogenic belt. It got transformed into an extensive fold-thrust belt as a result of the continental collision between Indian and Asian plate during the Cenozoic Himalayan orogeny[1–5]. The basal part of the Tethys Himalaya is commonly known as the Haimanta Group of rocks, whereas the upper part of the THS remains unmetamorphosed, and is commonly designated as Tethys Sedimentary Sequence (TSS). Studies show that the Haimanta Group of rocks has attained Cenozoic greenschist- to amphibolite-facies metamorphism[3,4,6–11]. The THS has also witnessed two major tectonic events: (i) the intrusion of Lower Palaeozoic granites of ~480–520 Ma often correlated with Pan-African orogeny and (ii) the tourmaline-bearing leucogranite emplacement during the Himalayan orogenic event at ~20–22 Ma.

Despite the occurrence of low-grade nature of metamorphic rocks in the Lahaul area, the chlorite–biotite grade Haimanta Group of rocks of the THS is important to understand the tectono-metamorphic evolution of the

*For correspondence. (e-mail: satya_edu1974@yahoo.co.in)

Himalayan orogeny[4,6,7,11]. Here we discuss the metamorphic evolution of garnet-grade rocks from in and around the Jaspa granite pluton. The *P–T* estimates are integrated to interpret the metamorphic evolution of the Tethys Himalaya of the Lahaul region in NW Himalaya, India and also throw light on the Himalayan versus pre-Himalayan nature of metamorphism, and the distribution of metamorphic geothermal gradient in the Tethys Himalaya.

Figure 1 shows the geological map of the Lahaul area, Himachal Pradesh (HP), India. The map is dominantly comprised of Haimanta Group of rocks, grouped into three formations – the older Batal Formation, the intermediate Kunjam La Formation and the younger Thange Formation (Figure 1 *b*). These rocks have been reported to have attained a low-grade chlorite–biotite zone of metamorphism[4,7,11], whereas the TSS remains unmetamorphosed[3]. On the other hand, the exposed sequence of rocks along the Keylong–Darcha transect has undergone biotite-grade of metamorphism[7], while the high-grade metamorphic rocks of the Higher Himalayan Crystalline Sequence (HHCS) are outcropped in the southeastern part of the Khoksar–Rohtang transect[4,10]. Figure 1 *a* shows the Zanskar HHCS that is exposed far northwest of the Jaspa granite pluton[4,6].

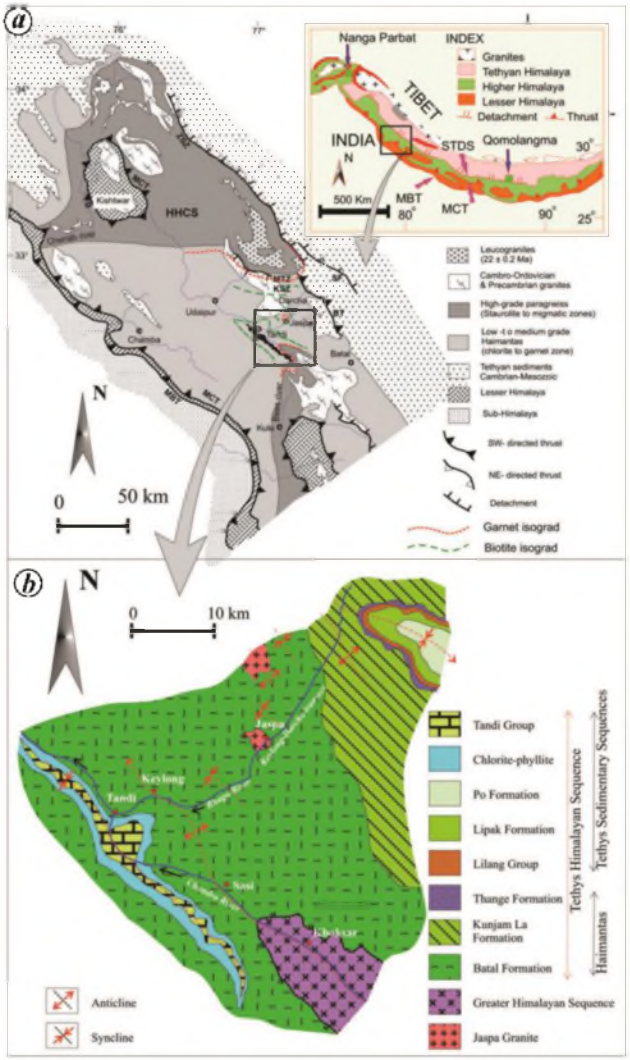

Figure 1. ***a***, Geological map of NW Himalaya (after Robyr *et al.*[4] and references therein) showing a generalized garnet and biotite isograd pattern in the study area (after Steck *et al.*[3], Webb *et al.*[10] and the present study). (Inset) Generalized map of the Himalaya; ***b***, Geological map of Lahaul area, Himachal Pradesh (after Srikantia and Bhargava[26]).

The Jaspa granite pluton is exposed in the Keylong–Darcha route along the Bhaga River, which is a tributary of the Chandra-Bhaga River in Lahaul area (Figure 1 *b*). The granite is outcropped as a sheet-like kilometre-scale plutonic body characterized by its coarse- to medium-grained porphyritic texture. The granite has intruded the Proterozoic rocks of Tethys Himalaya belonging to the Batal Formation of Haimanta Group during the Ordovician period (Figure 1 *b*). Pognante *et al.*[12] studied the rocks exposed to the northwest of Darcha and called them as the orthogneiss of Kade unit, and reported an age of ~549 ± 79 Ma. According to Thakur[13], the lithology of Kade unit partly corresponds to 'Chail–Haimanta' cover.

The Jaspa pluton encloses genetically related magmatic enclaves ranging in size from a few centimetres to tens of centimetres sporadically distributed in the Jaspa granite (Figure 2 *a*), and readily differentiated from the host granite pluton by its melanocratic appeal and relatively high amount of biotite. The boundary between magmatic enclaves and host granite is, however, defused. The Jaspa pluton also encloses the rare pelitic xenoliths of THS rocks. Pelitic xenoliths (i.e. metasedimentary rocks) show bedding, and have a sharp contact with the host granite pluton (Figure 2 *b*). The pelitic xenoliths belong to the Batal Formation of Haimanta Group, the dimension of which ranges between a few centimetres and tens of centimetres.

The magmatic enclaves and pelitic xenoliths are observed to possess the mineral assemblage that includes: bt–ms–pl–qz–tur ± grt ± kfs ± chl ± ep ± spn ± ilm ± ap. Table 1 shows the mineral assemblages observed in magmatic enclaves, pelitic xenolith and adjacent host granite. Anhedral to euhedral-shaped garnets are observed in two samples; one each from magmatic enclave (Figure 2 *c*; sample no. X-2) and pelitic xenolith (Figure 2 *d*; sample no. X-4). Among these, relatively larger garnets are commonly anhedral in shape, whereas small garnets are euhedral. The garnets are mostly inclusion-free, and if present are randomly oriented quartz with minor opaques. The chemical composition of garnet shows that it is rich in spessartine and grossular content (Table 2). Garnet of pelitic xenolith (sample X-4) is chemically homogenous, and the garnet of magmatic enclave (sample X-2) is chemically zoned, in which the spessartine and grossular contents increase, whereas almandine and pyrope contents decrease from core to rim (Table 2).

Table 1. Mineral assemblage of magmatic enclaves, pelitic xenoliths and host granite samples. Quartz is present in all samples (* indicates presence of minerals and blank indicates their absence). Mineral abbreviations used in the table and text are after Whitney and Evans[27]

Sample no.	Grt	Bt	Ms	Pl	Kfs	Chl	Ep	Spn	Ilm	Ap	Tur
Magmatic enclave samples											
X-1		*	*	*	*		*			*	
X-2	*	*	*	*			*	*			*
X-3		*	*	*			*				
X-5		*	*	*				*	*		
Pelitic xenolith sample											
X-4	*	*	*	*	*		*	*			*
Host granite samples											
H-1		*	*	*	*		*	*	*		
H-2		*	*	*	*		*				*
H-3		*	*	*	*	*	*	*		*	
H-4		*	*	*	*		*				
H-5		*	*	*	*		*	*		*	

The pelitic xenolith and host granite samples essentially contain both plagioclase and K-feldspar, whereas the magmatic enclaves possess plagioclase and are devoid of K-feldspar. Most of the plagioclases have undergone alteration and have a dusty appearance under the microscope. Some of them show intense alteration to sericite.

The magmatic enclaves, pelitic xenoliths and host granite show evidence of deformation as exhibited by few folded primary biotite flakes. The biotite is also seen altering into secondary biotite with no cleavage (Figure 2 *c*), contrary to one set of cleavage shown by the primary biotite. Muscovite is mostly secondary and it grows ubiquitously, commonly cross cutting the secondary biotite; however, a few of them are deformed and show prominent cleavage, suggesting their primary nature. The biotite and muscovite of pelitic xenolith are broadly aligned parallel to the schistosity (Figure 2 *e*). In general, the chemical composition of plagioclase, K-feldspar, muscovite, epidote, ilmenite and tourmaline is broadly similar both in magmatic enclaves and pelitic xenolith (Table 2), as well as in the host granite samples.

Further, the magmatic enclaves, pelitic xenolith and host granite samples have sphene (titanite). This occurs either as equidimensional individual grain or in the form of aggregates, or sometimes it occurs in the form of needles within biotite (Figure 2 *f*). The composition of sphene occurring in the matrix and in biotite (as inclusion) is more or less similar. Corona of sphene is also observed around ilmenite within the biotite (Figure 2 *g*). The occurrence of such textures indicates that the rocks have attained the low-grade metamorphic condition.

Epidote, another common accessory mineral after sphene, occurs as aggregates or as solitary grains scattered in the matrix; this also grows over the biotite. The magmatic enclaves, pelitic xenoliths and host granite samples are tourmaline-bearing (Figure 2 *c* and *d*). In one of the pelitic xenolith samples, tourmaline occurs in contact with garnet (Figure 2 *h*), indicating the coeval development of both minerals. Small chlorite grain is observed in one of the granite samples, indicating that the granite pluton has undergone a small degree of retrogression.

To understand the metamorphic conditions of rocks, the core and rim compositions of the garnet-bearing samples, X-2 (magmatic enclave) and X-4 (pelitic xenolith) were considered for *P–T* estimation using geothermobarometers. Table 3 lists the garnet, biotite and plagioclase solution models used in different calibrations. The garnet–biotite pair of sample X-2 yields metamorphic temperatures in the 409–531°C range, whereas for sample X-4 it is 376–451°C. Garnet core composition for both samples (i.e. X-2 and X-4) yields higher metamorphic temperature compared to rim composition, except for the calibration of Dasgupta *et al.*[14] for the magmatic enclave sample, which gave similar temperature values for core and rim compositions of the garnet (Table 3). The pressure estimates show that the rocks have attained metamorphic pressure in a range 5.7–8.6 kbar. The metamorphic pressure estimated considering the core composition of the garnet is relatively high compared to the rim composition for both the samples, which indicates that rocks underwent burial with cooling during their metamorphic evolution. The *P–T* estimates thus obtained from various geothermobarometry calibrations show that the Tethys Himalayan rocks in and around the Jaspa granite have attained peak metamorphic temperature in a range ~400–531°C and pressure in the range ~5.7–8.6 kbar (Table 3).

The *P–T* pseudosection (Figure 3) has also been constructed for bulk rock composition (XRF data) of one of the magmatic enclave samples (X-2) considering the model chemical system – MnNCKFMASHT using the PERPLEX_6.7.2 software[15,16] and end-member thermodynamic dataset of Holland and Powell[17] (updated in 2004). For the pseudosection modelling, quartz is chosen as an excess phase. A correction in CaO to the bulk rock is made assuming total P_2O_5 to be present only in apatite. All iron has been considered as ferrous assuming that the ferric iron has the least influence on the *P–T* stability field of different phase assemblages. The grt–bt–ms–ep–

Table 2. Representative electron microprobe analyses of garnet-bearing magmatic enclave (X-2) and pelitic xenolith sample (X-4)

	Magmatic enclave sample X-2									Pelitic xenolith sample X-4							
	Grt core	Grt rim	Bt	Ms	Ep	Pl	Spn	Tur	Grt core	Grt rim	Bt	Ms	Ep	Pl	Kfs	Spn	Tur
SiO_2	36.80	37.40	36.56	47.98	37.04	62.76	30.57	36.85	37.95	37.73	36.59	47.66	38.35	65.28	64.49	30.82	35.80
TiO_2	0.08	0.09	1.64	0.05	0.10	b.d.	34.43	b.d.	0.14	0.02	1.09	0.29	0.09	b.d.	0.03	31.57	0.99
Al_2O_3	20.66	20.80	16.78	29.92	24.04	21.43	3.49	33.37	20.99	20.95	17.25	28.91	27.31	21.48	18.24	5.21	33.44
FeO	32.80	14.65	19.55	3.48	9.61	1.49	0.66	6.71	14.50	16.01	21.41	4.05	6.59	0.14	0.02	0.40	7.78
MnO	5.64	11.81	0.49	0.05	0.36	0.02	0.13	0.08	10.38	11.43	0.46	0.16	0.28	b.d.	0.01	0.10	0.09
MgO	1.90	0.37	8.73	2.01	0.03	0.66	0.03	6.67	0.31	0.31	8.16	2.23	0.03	b.d.	0.01	b.d.	4.56
CaO	1.37	14.53	0.01	0.02	22.74	1.81	28.57	0.67	15.46	13.42	0.04	b.d.	23.22	2.88	0.00	28.47	0.52
Na_2O	0.04	0.01	0.15	0.31	0.04	9.40	0.03	2.06	0.01	0.01	0.14	0.16	0.01	10.05	0.70	0.04	1.94
K_2O	b.d.	b.d.	9.96	11.20	0.06	1.64	0.07	0.02	b.d.	0.02	8.74	10.52	0.03	0.11	14.93	0.03	0.01
Total	99.29	99.66	93.87	95.02	94.02	99.21	97.98	86.43	99.74	99.90	93.88	93.98	95.91	99.94	98.43	96.64	85.13
Oxygen basis	12	12	22	22	13	8	20	31	12	12	22	22	13	8	8	20	31
Si	3.008	2.989	5.672	6.495	3.216	2.821	4.059	7.562	3.012	3.009	5.682	6.521	3.200	2.875	3.004	4.124	7.494
Ti	0.005	0.005	0.191	0.005	0.007	0.000	3.438	0.000	0.008	0.001	0.127	0.030	0.006	0.000	0.001	3.177	0.156
Al	1.991	1.959	3.068	4.774	2.460	1.135	0.546	8.071	1.964	1.969	3.157	4.662	2.685	1.115	1.002	0.822	8.250
Fe	2.242	0.979	2.537	0.394	0.698	0.056	0.073	1.152	0.963	1.068	2.780	0.463	0.460	0.005	0.001	0.045	1.362
Mn	0.391	0.799	0.064	0.006	0.026	0.001	0.015	0.014	0.698	0.772	0.061	0.019	0.020	0.000	0.000	0.011	0.016
Mg	0.232	0.044	2.019	0.406	0.004	0.044	0.006	2.040	0.037	0.037	1.889	0.455	0.004	0.000	0.001	0.000	1.423
Ca	0.120	1.244	0.002	0.003	2.116	0.087	4.064	0.147	1.315	1.147	0.007	0.000	2.076	0.136	0.000	4.082	0.117
Na	0.006	0.002	0.045	0.081	0.007	0.819	0.008	0.820	0.002	0.002	0.042	0.042	0.002	0.858	0.063	0.010	0.787
K	0.000	0.000	1.971	1.934	0.007	0.094	0.012	0.005	0.000	0.002	1.731	1.836	0.003	0.006	0.887	0.005	0.003
Total	7.995	8.022	15.570	14.098	8.540	5.057	12.221	19.812	7.998	8.007	15.475	14.029	8.454	4.996	4.959	12.276	19.607
X_{Fe}	0.91	0.96	0.56	0.49	0.99		0.93	0.36	0.96	0.97	0.60	0.50	0.99			1.00	0.49
X_{alm}	0.75	0.32							0.32	0.35							
X_{prp}	0.08	0.01							0.01	0.01							
X_{grs}	0.04	0.41							0.44	0.38							
X_{sps}	0.13	0.26							0.23	0.26							
X_{an}						0.09								0.14	0.00		
X_{ab}						0.82								0.86	0.07		
X_{or}						0.09								0.01	0.93		

X_{Fe} = Fe/(Fe + Mg); X_{alm} = Fe/(Fe + Mg + Ca + Mn); X_{prp} = Mg/(Fe + Mg + Ca + Mn); X_{sps} = Mn/(Fe + Mg + Ca + Mn); X_{grs} = Ca/(Fe + Mg + Ca + Mn); X_{an} = Ca/(Ca + Na + K); X_{ab} = Na/(Ca + Na + K); X_{or} = K/(Ca + Na + K).

b.d. = below the detection limit; Detection limit for elemental oxides is <0.01 wt% (except FeO = <0.02 wt%).

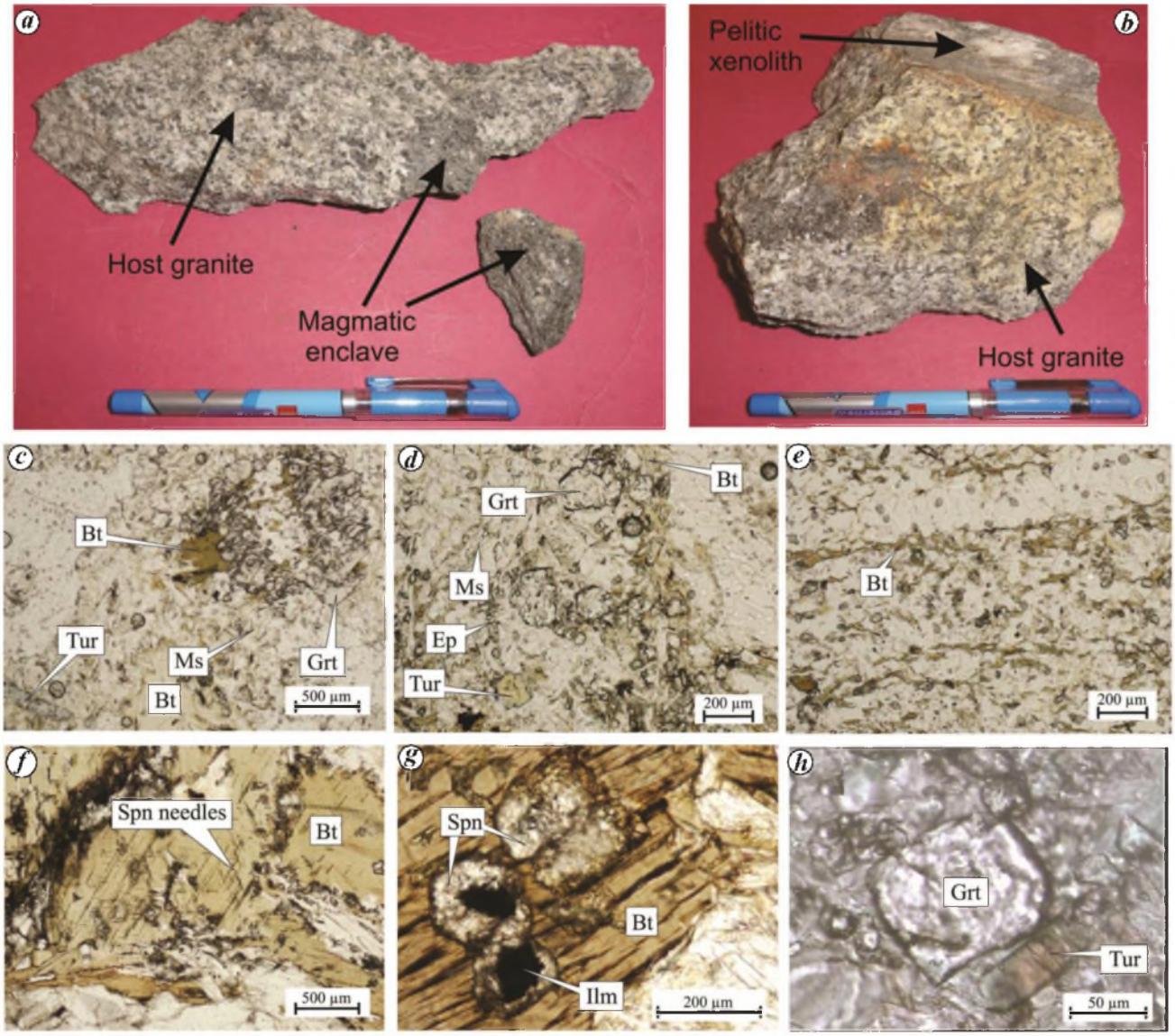

Figure 2. Photographs of hand specimens and photomicrographs of selected samples from the study area. ***a***, Photograph showing magmatic enclave associated with the host Jaspa granite (sample X-2 and H-2). ***b***, Photograph of pelitic xenolith showing sharp contact with the host Jaspa granite (sample X-4 and H-4); one can also observe pelitic xenolith at the top showing primary bedding feature with quartz-rich bands. ***c***, Photomicrograph of magmatic enclave sample X-2 showing mineral assemblage: ms–bt–grt–pl–qz–tur, and a large altered biotite at the centre (under plane polarized light). ***d***, Photomicrograph of pelitic xenolith sample X-4 showing mineral assemblage: ms–bt–grt–pl–qz–ep–tur, and a high relief prismatic epidote at the centre (under plane polarized light). ***e***, Photomicrograph showing biotite flakes aligned parallel to the bedding plane; the light-coloured minerals are mostly quartz (sample X-4). ***f***, Photomicrograph showing high-relief, needle-shaped grains of sphene (titanite) as inclusion in biotite (sample H-1). ***g***, Photomicrograph showing sphene coronae around ilmenite within biotite (sample X-5). ***h***, Photomicrograph showing coexisting garnet and tourmaline grains (sample X-4).

pl–spn–qz–kfs is the characteristic mineral assemblage in this sample (X-2). The pseudosection shows that this assemblage is stable in a narrow P–T stability field range of ~4.5–7.3 kbar and ~440–500°C. The P–T pseudosection modelling shows that the assemblage was developed from the chl–kfs–spn–ep bearing low P–T assemblages with increasing metamorphic grade, with a Barrovian trend of metamorphic field gradient of 25–35°C/km. Garnet and epidote appear in the rock at ~3.5 kbar and ~350°C, while chlorite gets exhausted with increasing P and T, and disappears from the rock at ~4.0 kbar and ~390°C along the predetermined metamorphic field gradient.

There are reports of the occurrence of pre-Himalayan metamorphism in the Himalayan Orogenic belt[13,18–21]. In Lahaul area, the lower Palaeozoic magmatic activity resulted in the formation of Jaspa granite pluton[22], which is being correlated with the Pan-African orogeny. However, the present study shows that the garnet was formed during the Cenozoic metamorphism, during or after the emplacement of tourmaline-bearing leucogranite. A clear

Table 3. *P–T* estimates for garnet-bearing magmatic enclave sample X-2 and pelitic xenoliths sample X-4

	Grt solution model	Bt/Pl solution model	X-2 (grt core)	X-2- (grt rim)	X-4 (grt core)	X-4 (grt rm)
Grt–Bt geothermometer* (°C)						
Calibration						
Hodges and Spear[28]	Fe–Mg–Ca–Mn, non-ideal mixing	Fe–Mg–Al–Ti, ideal mixing in bt	501	444	451	417
Perchuk and Lavrent'eva[29]	Fe–Mg–Mn, ideal mixing	Fe–Mg–Mn, ideal mixing in bt	531	410	409	398
Ganguly and Saxena[30]	Fe–Mg–Ca–Mn, non-ideal mixing	Fe–Mg, ideal mixing in bt	528	445	446	425
Dasgupta *et al.*[14]	Fe–Mg–Ca–Mn, non-ideal mixing	Fe–Mg–Al–Ti non-ideal mixing in bt	409	410	409	376
Geobarometer (GPBMQ)** (kbar)						
Calibration						
Ghent and Stout[31]–Fe	Fe–Mg–Ca–Mn, ideal mixing	Na–Ca–K ideal mixing in Pl, Fe–Mg–Mn–Ti–Al^{VI} ideal mixing in bt	5.8	8.6	8.4	7.8
Ghent and Stout[31]–Mg	Fe–Mg–Ca–Mn, ideal mixing	Na–Ca–K ideal mixing in Pl, Fe–Mg–Mn–Ti–Al^{VI} ideal mixing in bt	5.7	7.6	6.8	6.4
Hodges and Crowley[32]–Fe	Fe–Mg–Ca–Mn, ideal mixing	Na–Ca ideal mixing in Pl, Fe–Mg–Ti–Al^{VI} ideal mixing in bt	5.7	7.9	7.7	6.8

*Temperature calculated at 8 kbar pressure.
**Pressure calculated at temperature value obtained from Hodges and Spear[28].

evidence of Himalayan metamorphism in the Tethys Himalayan rocks of Lahaul region is thus observed. For example, garnet has been seen growing in the pelitic xenolith characterized by the presence of sedimentary bedding plane structure (Figure 2 *b*), the occurrence of tourmaline in xenoliths (Figure 2 *c*, *d* and *h*) as well as in host rocks, indicating that they have undergone Himalayan metamorphism during the Cenozoic; and the presence of coexisting garnet and tourmaline (Figure 2 *h*) further suggests that the garnet-grade metamorphism in the Jaspa area is the result of Himalayan Cenozoic metamorphism.

Moreover, if one considers the metamorphic field gradient and from the tectonics point of view, it is seen that there are mainly two high-grade metamorphic domains exposed around the study area: the first one is the Zanskar HHCS exposed in the northwest of the Jaspa granite pluton[4,6] and other is the HHCS of Khoksar–Rohtang crystallines in the south–southeast of the Jaspa pluton[10,11] (Figure 1 *a*). Comparison of the *P–T* conditions of metamorphism of the Jaspa granite with those of the HHCS crystallines shows that the Jaspa granite has reached peak metamorphic *P–T* condition of ~400–531°C and 5.7–8.6 kbar, whereas the HHCS rocks have attained the metamorphic *P–T* condition of ~500–635°C and 4.7 to 6.8 kbar in Kullu–Rohtang[23]; ~650–780°C in the Rohtang–Khoksar area[10,11] and around ~750–850°C in the Zanskar Himalaya[4,6]. The presence of garnet-grade metamorphic rocks in and around the Jaspa pluton located between the Zanskar crystalline and Khoksar–Rohtang crystalline suggests that, during Cenozoic Himalayan tectono-thermal event, the isotherm probably perturbed slightly upward causing localized garnet-grade metamorphism in the area. The *P–T* results considering the core and rim compositions of garnet further suggest that the terrain underwent burial with cooling metamorphic history after reaching the peak *P–T* conditions of metamorphism. Presence of intrusive Miocene leucogranite within the Jaspa granite in the study area suggests that such burial and cooling metamorphism is due to cooling of the terrain with the burial of Tethys Himalayan rocks after the leucogranite emplacement. This is well supported by several studies that advocate the anticlockwise *P–T* path in the orogenic belt associated with igneous intrusion[24,25]. The metamorphism shows a gradual decrease from the sil/ky grade to the chlorite–biotite grade outward from the crystalline core of the Zanskar shear zone in Zanskar area[6]. This suggests that the Zanskar crystalline shows a gradual decrease of metamorphic grade from sillimanite grade at the crystalline core to biotite grade towards the east, prior to reaching the Jaspa granite[10], and then increases to garnet grade in and around the Jaspa granite (Figure 1 *a*). The metamorphic grade gradually decreases further from the Jaspa pluton to the Tandi syncline towards the south where it reaches the chlorite–biotite grade[3] and then gradually increases toward Khoksar–Rohtang Higher Himalayan crystalline (Figure 1 *a*). Such a metamorphic trend indicates that the Tethys Himalaya in the study region shows right-way-up metamorphic field gradient, an inference which is consistent with the observation made by Leger *et al.*[11] in the Beas River Valley, NW Himalaya, south of the study area.

The *P–T* pseudosection modelling and the *P–T* estimates obtained from conventional geothermobarometry method show that the Tethys Himalayan rocks exposed in and around the Jaspa granite have undergone peak

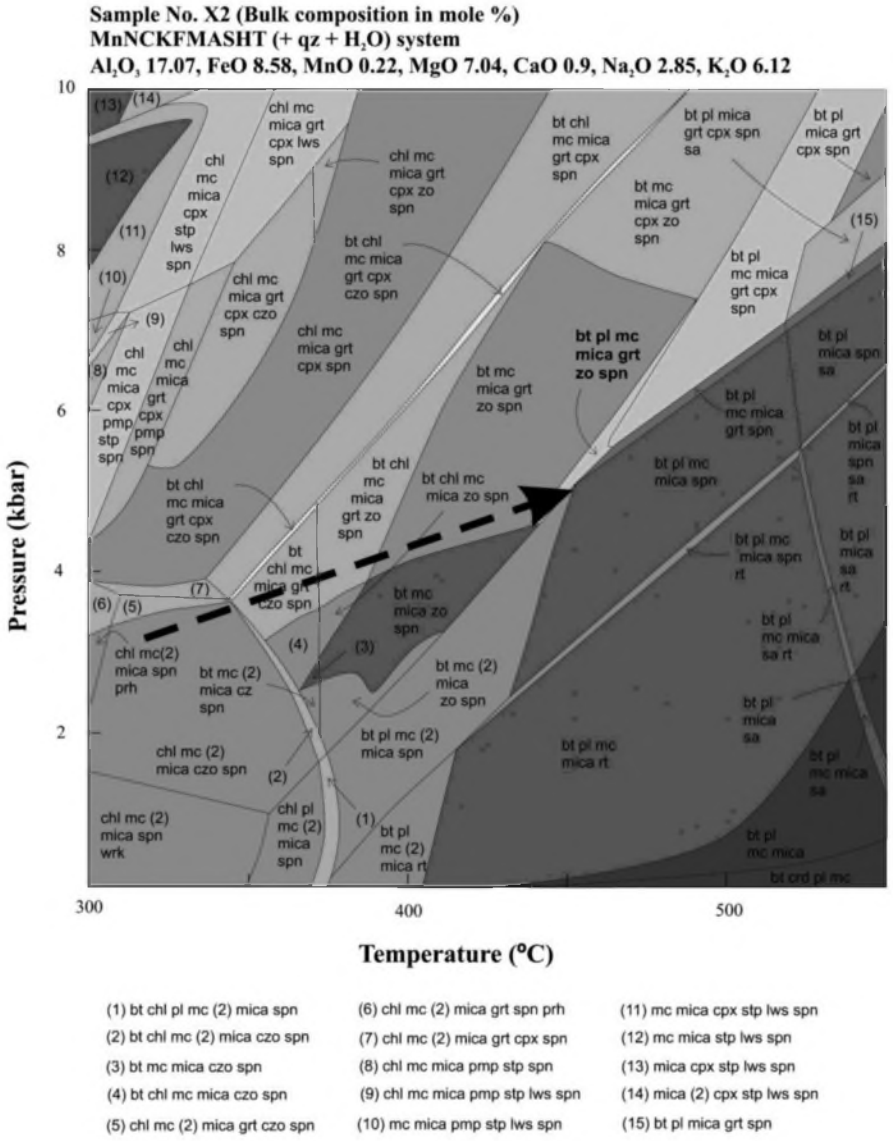

Figure 3. *P–T* pseudosection in the MnNCKFMASHT system (+quartz + H_2O) at $\alpha_{H_2O} = 1$ considering fixed bulk rock composition for sample X-2. The stability field of mineral assemblage is shown in bold. An arrow is drawn considering the metamorphic field gradient of 30°/km, indicating that the assemblage of sample X-2: grt–bt–ms–ep–pl–sph–qz–kfs has formed from the chl–kfs–spn–ep-bearing low *P–T* assemblages. Details of solid solutions, phases and end-members used in *P–T* pseudosection modelling are given in the supplementary material.

metamorphic temperature conditions in the range 400–531°C and pressure in the range 5.7–8.6 kbar. The metamorphic study of magmatic enclaves and pelitic xenolith embedded in the Jaspa granite further shows that they have undergone garnet-grade Cenozoic metamorphism due to localized perturbation of high-temperature isotherms in the Tethys Himalaya, and that the Tethys Himalaya in the study area shows right way-up metamorphic field gradient, consistent with observations in the Beas River valley lying south of the study area.

1. Gansser, A., *The Geology of the Himalaya*, Wiley Inter-science, New York, 1964.
2. LeFort, P., Himalayas: the collided range. Present knowledge of the continental arc. *Am. J. Sci.*, 1975, **275**A, 1–44.
3. Steck, A. *et al.*, Geological transect across the Northwestern Himalaya in eastern Ladakh and Lahul (a model for the continental collision of India and Asia). *Eclogae Geol. Helv.*, 1993, **86**, 219–263.
4. Robyr, M., Hacker, B. R. and Mattinson, J. M., Doming in compressional orogenic settings: new geochronological constraints from the NW Himalaya. *Tectonics*, 2006, **25**, TC2007; doi:10.1029/2004TC001774.
5. Yin, A., Cenozoic tectonic evolution of the Himalayan orogen as constrained by along strike variation of structural geometry, exhumation history, and foreland sedimentation. *Earth Sci. Rev.*, 2006, **76**, 1–131.
6. De`zes, P. J., Vannay, J. C., Steck, A., Bussy, F. and Cosca, M., Synorogenic extension: quantitative constraints on the age and

displacement of the Zanskar shear zone (northwest Himalaya). *Geol. Soc. Am. Bull.*, 1999, **111**, 364–374.
7. Walker, J. D., Martin, M. W., Bowring, S. A., Searle, M. P., Waters, D. J. and Hodges, K. V., Metamorphism, melting, and extension: age constraints from the High Himalayan Slab of southeast Zanskar and northwest Lahul. *J. Geol.*, 1999, **107**, 473–495.
8. Thakur, S. S. and Tripathi, K., Regional metamorphism in the Haimanta Group of rocks, Sutlej river valley, NW Himalaya. *Curr. Sci.*, 2008, **95**, 104–109.
9. Chambers, J. *et al.*, Empirical constraints on extrusion mechanisms from the upper margin of an exhumed high-grade orogenic core, Sutlej valley, NW India. *Tectonophysics*, 2009, **477**, 77–92.
10. Webb, A. A. G., Yin, A., Harrison, T. M., Celerier, J., Gehrels, G. E., Manning, C. E. and Grove, M., Cenozoic tectonic history of the Himachal Himalaya (northwestern India) and its constraints on the formation mechanism of the Himalayan orogen. *Geosphere*, 2011, **7**, 1013–1061.
11. Leger, R. M., Webb, A. A. G., Henry, D. J., Craig, J. A. and Dubey, P., Metamorphic field gradients across the Himachal Himalaya, northwest India: implications for the emplacement of the Himalayan crystalline core. *Tectonics*, 2013, **32**, doi:10.1002/tect.20020.
12. Pognante, U., Castelli, D., Benna, P., Genovese, G., Oberli, F., Meier, M. and Tonarini, S., The crystalline units of the High Himalayas in the Lahul–Zanskar region (northwest India): metamorphic–tectonic history and geochronology of the collided and imbricated India plate. *Geol. Mag.*, 1990, **127**, 101–116.
13. Thakur, V. C., Tectonics of the central crystallines of western Himalaya. *Tectonophysics*, 1980, **62**, 141–154.
14. Dasgupta, S., Sengupta, P., Guha, D. and Fukuoka, M., A refined garnet – biotite Fe–Mg exchange geothermometer and its application in amphibolites and granulites. *Contrib. Mineral. Petrol.*, 1991, **109**, 130–137.
15. Connolly, J. A. D., Multivariable phase diagram: an algorithm based on generalized thermodynamics. *Am. J. Sci.*, 1990, **290**, 666–718.
16. Connolly, J. A. D., Computation of phase equilibria by linear programming: a tool from geodynamic modelling and its application to subduction zone decarbonation. *Earth Planet. Sci. Lett.*, 2005, **236**, 524–541.
17. Holland, T. J. B. and Powell, R., An internally consistent thermodynamic dataset for phases of petrological interest. *J. Metamorph. Geol.*, 1998, **16**, 309–344.
18. Marquer, D., Chawla, H. S. and Challandes, N., Pre-alpine high-grade metamorphism in high Himalaya crystalline sequences: evidence from Lower Palaeozoic Kinnaur Kailash Granite and surrounding rocks in Sutlej Valley (Himachal Pradesh, India). *Eclogae Geol. Helv.*, 2000, **93**, 207–220.
19. Gehrels, G. E., DeCelles, P. G., Martin, A., Ojha, T. P. and Pinhassi, G., Initiation of the Himalayan orogen as an early Palaeozoic thin-skinned thrust belt. *GSA Today*, 2003, **13**, 4–9.
20. Thakur, S. S., Retrograde corona texture in pre-Himalayan metamorphic mafic xenoliths, Sutlej valley, NW Himalaya: implication on rare occurrence of high-grade rocks in the Himalaya. *J. Asian Earth Sci.*, 2014, **88,** 41–49.
21. Thakur, S. S. and Patel, S. C., Mafic and pelitic xenoliths in the Kinnaur Kailash Granite, Baspa river valley, NW Himalaya: evidence of pre-Himalayan granulite metamorphism followed by cooling event. *J. Asian Earth Sci.*, 2012, **56,** 105–117.
22. Rameshwar Rao, D. and Sharma, K. K., Petrological and geochemical constraints on the petrogenesis of the Jaspa granite pluton, Lahual region, NW Himalaya. *J. Geol. Soc. India*, 1995, **45**, 629–642.
23. Rameshwar Rao, D. and Gururajan, N. S., Metamorphism of the inverted sequence in Himachal Himalaya: a study from the Kullu–Rohtang–Khoskar section. *J. Geol. Soc. India*, 2000, **56**, 633–649.
24. Sandiford, M., Martin, N., Zhou, S. and Fraser, G., Mechanical consequences of granite emplacement during high-*T*, low-*P* metamorphism and the origin of 'anticlockwise' *PT* paths. *Earth Planet. Sci. Lett.*, 1991, **107**, 164–172.
25. Sandiford, M. and Powell, R., Some remarks on high-temperature–low-pressure metamorphism in convergent orogens. *J. Metamorph. Geol.*, 1991, **9**, 333–340.
26. Srikantia, S. V. and Bhargava, O. N., The Tandi Group of Lahaul: its geology and relationship with the Central Himalayan gneiss. *J. Geol. Soc. India*, 1979, **20**, 531–539.
27. Whitney, D. L. and Evans, B. W., Abbreviations for names of rock-forming minerals. *Am. Mineral.*, 2010, **95**, 185–187.
28. Hodges, K. V. and Spear, F. S., Geothermometry, geobarometry and the Al_2SiO_5 triple point at Mt. Moosilauke, New Hampshire. *Am. Mineral.*, 1982, **67**, 1118–1134.
29. Perchuk, L. L. and Lavrent'eva, I. V., Experimental investigation of exchange equilibria in the system cordierite–garnet–biotite. In *Kinetics and Equilibrium in Mineral Reactions* (ed. Saxena, S. K.), Springer-Verlag, New York, 1983, pp. 199–239.
30. Ganguly, J. and Saxena, S. K., Mixing properties of aluminosilicate garnets. Constraints from natural and experimental data and applications to geothermobarometry. *Am. Mineral.*, 1984, **69**, 88–97.
31. Ghent, E. D. and Stout, M. Z., Geobarometry and geothermometry of plagioclase–biotite–garnet–muscovite assemblages. *Contrib. Mineral. Petrol.*, 1981, **76**, 92–97.
32. Hodges, K. V. and Crowley, P. D., Error estimation and empirical geothermometry for pelitic system. *Am. Mineral.*, 1985, **70**, 702–709.

ACKNOWLEDGEMENTS. We thank Dr Meera Tiwari (Director (Additional Charge), Wadia Institute of Himalayan Geology, Dehradun) for providing laboratory facilities and permission to publish this work. We also thank Prof. N. V. Chalapathi Rao (Banaras Hindu University, Varanasi) for editorial handling; an anonymous reviewer for constructive comments on the manuscript; and Mr Chandra Shekhar (Wadia Institute of Himalayan Geology, Dehradun) for generating the XRF data. S.P. thanks CSIR, New Delhi for JRF fellowship. The mineral chemical analyses were carried out using a CAMECA SX100 electron microprobe (EPMA) at the Wadia Institute of Himalayan Geology, Dehradun, with an acceleration voltage of 15 kV, beam current of 20 nA and beam diameter of 1 μm. Both natural and synthetic standards were used. The raw data were corrected using the PAP program.

Received 18 December 2017; revised accepted 30 April 2018

doi: 10.18520/cs/v115/i8/1576-1583